Biomedicine & Pharmacotherapy 166 (2023) 115312

Contents lists available at ScienceDirect

Biomedicine & Pharmacotherapy

journal homepage: www.elsevier.com/locate/biopha

Development of a novel histone deacetylase inhibitor unveils the role of HDAC11 in alleviating depression by inhibition of microglial activation

Soo Yeon Baek [a,1], Jeehee Lee [a,b,1], Taegwan Kim [c], Hyelim Lee [a], Hoon-Seong Choi [d], Hahnbeom Park [a], Minseob Koh [e], Eunha Kim [f], Michael E. Jung [g], Dimitrios Iliopoulos [h], Jeong-Yeon Lee [i], Jonghoon Kim [c,*], Sanghee Lee [a,b,**]

[a] Center for Brain Disorders, Brain Science Institute, Korea Institute of Science and Technology, Seoul 02792, South Korea
[b] Department of HY-KIST Bio-convergence, Hanyang University, Seoul 04763, South Korea
[c] Department of Chemistry and Integrative Institute of Basic Science, Soongsil University, Seoul 06978, South Korea
[d] Research Animal Resources Center, Research Resources Division, Korea Institute of Science and Technology, Seoul 02792, South Korea
[e] Department of Chemistry, Pusan National University, Busan 46241, South Korea
[f] Department of Molecular Science and Technology, Ajou University, Suwon 16499, South Korea
[g] Department of Chemistry & Biochemistry, University of California at Los Angeles (UCLA), Los Angeles, CA 90095-1569, USA
[h] Center for Systems Biomedicine, Vatche and Tamar Manoukian Division of Digestive Diseases, David Geffen School of Medicine, University of California at Los Angeles (UCLA), Los Angeles, CA 90095, USA
[i] Department of Pathology, College of Medicine, Hanyang University, Seoul 04763, South Korea

ARTICLE INFO

Keywords:
HDAC inhibitor
Microglial activation
Neuroinflammation
Depressive disorder

ABSTRACT

Histone deacetylases (HDACs) are key epigenetic regulators and classified into four subtypes. Despite the various roles of each HDAC isoform, the lack of selective HDAC inhibitors has limited the elucidation of their roles in biological systems. HDAC11, the sole class-IV HDAC, is highly expressed in the brain, however, the role of HDAC11 in microglia is not fully understood. Based on the modification of MC1568, we developed a novel HDAC inhibitor, **5**. Interestingly, **5** suppresses lipopolysaccharide-induced microglial activation by the initiation of autophagy and subsequent inhibition of nitric oxide production. Furthermore, we demonstrated that **5** significantly alleviates depression-like behavior by inhibiting microglial activation in mouse brain. Our discovery reveals that specific pharmacological regulation of HDAC11 induces autophagy and reactive nitrogen species balance in microglia for the first time, which makes HDAC11 a new therapeutic target for depressive disorder.

1. Introduction

Histone deacetylases (HDACs) are key epigenetic regulators that control DNA transcription and modulate cellular processes by deacetylating lysine residues on histones or non-histone proteins, such as various transcription factors, heat shock protein 90, signaling proteins, and tubulin [1]. In general, HDACs are divided into four classes based on their structure and function: class I (HDAC1, 2, 3, and 8), class II (further subdivided into IIa (HDAC4, 5, 7, and 9), and IIb (HDAC6 and 10)), class III (SIRT1–7), and class IV (HDAC11) [2].

Although HDACs are widely considered important therapeutic targets for various cancers [3], individual HDAC isoforms mediate different biological phenomena observed in diverse tissues and diseases. Class I HDACs regulate neuroinflammation and class II HDACs are related to stellate cell activation in the liver, renal fibrosis, neuronal cell death, and Parkinson's disease [4]. Regarding the function of HDACs in the brain, the inhibition of HDAC6 enhances autophagy and lysosomal function in mice with Cockayne syndrome [5]. HDAC1 and HDAC2 are responsible for the development of the cells and the maintenance of homeostasis in the central nervous system (CNS), which they achieve by

Abbreviations: HDACs, histone deacetylases; CNS, central nervous system; AD, Alzheimer's disease; VPA, valproic acid; TSA, trichostatin-A; SAHA, suberoylanilide hydroxamic acid; RNS, reactive nitrogen species; NO, nitric oxide; TMS, tetramethylsilane; TNF- α, tumor necrosis factor-α; iNOS, inducible nitric oxide synthase; LPS, lipopolysaccharide; TST, Tail Suspension Test; FST, Forced Swimming Test; SPT, Sucrose Preference Test.

* Corresponding author.
** Corresponding author at: Center for Brain Disorders, Brain Science Institute, Korea Institute of Science and Technology, Seoul 02792, South Korea.
E-mail addresses: jhkim19@ssu.ac.kr (J. Kim), slee19@kist.re.kr (S. Lee).
[1] These authors contributed equally.

https://doi.org/10.1016/j.biopha.2023.115312
Received 22 June 2023; Received in revised form 7 August 2023; Accepted 7 August 2023
Available online 9 August 2023

regulating microglia phagocytosis [6]. Microglia are brain-resident immune cells that mediate immune responses in the brain and sustain CNS homeostasis [7]. The depletion of HDAC1 and HDAC2 levels in an Alzheimer's disease (AD) mouse model increased the phagocytic activity of microglia, resulting in reduced AD pathology [6]. It is worth mentioning that these findings provide a new therapeutic strategy for AD associated with epigenetic mechanisms. Therefore, elucidating the novel role that HDACs play in various biological processes in microglia has rendered them attractive therapeutic targets.

HDAC11 is the only isoform in class IV; it is also the most recently identified and smallest HDAC enzyme [8]. HDAC11 is mainly expressed in the brain, testis, and immune cells, and plays important roles in tumorigenesis, immune response, and metabolism [9]. The anti-inflammatory effect of *pan*-HDAC inhibitors such as trichostatin-A (TSA) and suberoylanilide hydroxamic acid (SAHA) alleviate cognitive dysfunction and ischemia, respectively, by preventing microglia activation and inducing neuroprotection [10]. Regardless of these efforts, the cellular functions of individual HDACs in microglia are not fully understood; especially that of HDAC11, despite its high expression level in the brain.

To elucidate the specific modulation of particular HDAC isoforms and demonstrate their therapeutic potential, the discovery of selective HDAC inhibitors is important. Nevertheless, most *pan*-HDAC inhibitors, such as TSA, SAHA, and valproic acid (VPA), have been used since the 1990 s (Fig. 1A) [11]. To promote selective events, several inhibitors targeting specific HDAC classes have been developed and are commercially available: MS-275 for HDAC1, 2, and 3 (class I); MC1568 for class II HDACs; LMK-235 for HDAC4 and HDAC5; and ACY-1215 for HDAC1–3 and 6 [12]. However, only a few inhibitors of HDAC11 such as SIS17 and FT895 have been reported to date (Fig. 1A), despite notable advances in the discovery of selective HDAC inhibitors [13]. Unfortunately, the X-ray crystal structure of HDAC11 has not yet been characterized, which can limit the application of classic strategies such as target-based drug design for the development of new chemical entities. In addition, it has been reported that HDAC11 exhibits not only deacetylase activity but also potent defatty-acylase and de-myristoylation activities [14]. Even if it has a versatile function, the role of HDAC11 remains unknown owing to the lack of chemical tools for its biological evaluation.

In this study, we discovered an HDAC11 inhibitor, compound **5**, that clearly improved the potency of cellular-level *pan*-HDAC inhibition than MC1568 and modulated deacetylase function of HDAC11 in contrast to SIS17 (Fig. 1A). Interestingly, **5** regulated autophagy and reactive nitrogen species (RNS) system in microglia, that was not corresponding to the cellular *pan*-HDAC activity. We elucidated that the cellular phenotype induced by **5** corresponded to the *in vitro* HDAC11 inhibitory pattern. Therefore, our discovery of a new HDAC11 inhibitor unveiled the new role of HDAC11 which is significantly involved in autophagy and RNS production in microglia *via* its deacetylase function. Furthermore, we demonstrated the therapeutic potential of **5** by inhibition of HDAC11 to alleviate depression-like behavior in mice.

2. Materials and methods

2.1. Chemical synthesis

All commercially available reagents were used without further purification unless noted otherwise. Dried solvents and triethylamine (Et_3N) were passed through solvent purification systems equipped with activated alumina columns (Glass Contour). NMR analyses were carried out using Varian/Oxford As-500 (500 MHz; Varian Assoc., Palo Alto, USA) or Bruker AVANCE 600 (600 MHz; Bruker, Germany) spectrometers. The chemical shift values of the proton (^1H) and carbon (^{13}C) NMR spectra were reported in parts per million (δ), to the internal standard tetramethylsilane (TMS) or to the residual solvent peak ($CDCl_3$, ^1H: 7.26, ^{13}C: 77.16; DMSO-d_6, ^1H: 2.50, ^{13}C: 39.52). The multiplicities of the ^1H NMR peaks are reported as follows: s (singlet), d (doublet), t (triplet), q (quartet), m (multiplet), dd (doublet of doublets), dt (doublet of triplets), td (triplet of doublets), and br s (broad singlet). The coupling constants (J) were reported in Hz. Low-resolution mass spectrometry (LRMS) spectra were obtained on an LCMS-2020 spectrometer (Shimadzu, Japan) using the electrospray ionization (ESI) method. High-resolution mass spectra were analyzed using the ESI mode of an LCQ LC/MS spectrometer (Thermo Fisher Scientific, USA). To monitor the progress of the reactions, analytical thin-layer chromatography (TLC) analysis was performed using glass plates precoated with silica gel (60 F254, Merck, Germany), and the components were observed under UV light (254 and 365 nm). Flash column chromatography was performed using silica gel 60 (230–400 mesh, Merck, Germany).

2.2. Cell culture

HMC3 cells were cultured in Dulbecco's modified Eagle's medium (DMEM) supplemented with 10% (v/v) heat-inactivated fetal bovine serum (FBS; Hyclone) and 1% (v/v) antibiotic-penicillin solution (Corning). HMO6 and BV-2 cells were cultured in DMEM supplemented with 10% (v/v) heat-inactivated FBS (Gibco), 1% (v/v) antibiotic-penicillin solution, and 0.1% (v/v) anti-mycoplasma solution. HeLa cells were obtained from KCCB and cultured in RPMI 1640 supplemented with 10% (v/v) heat-inactivated FBS (Hyclone) and 1% (v/v) antibiotic-penicillin solution. The cells were incubated at 37 °C in a 5% CO_2 incubator under a humidified atmosphere.

2.3. Cell-based HDAC activity assay

Nuclear extraction was performed using a NE-PER nuclear cytoplasmic extraction reagent kit (Pierce) according to the manufacturer's instructions. Briefly, the cell pellet was suspended in 200 μL of cytoplasmic extraction reagent by vortexing. The suspension was incubated on ice for 10 min, followed by the addition of 11 μL of a second cytoplasmic extraction reagent, vortexed for 5 s, incubated on ice for 1 min, and finally centrifuged for 5 min at 16,000g. The insoluble pellet fraction, which contained crude nuclei, was resuspended in 100 μL of nuclear extraction reagent by vortexing for 15 s, incubated on ice for 10 min, and then centrifuged for 10 min at 16,000g. The constituting nuclear extract was used for the HDAC activity assay using a fluorometric assay kit (Enzo) according to the manufacturer's protocol. In brief, assays were performed with HDAC inhibitors in 10 μL of an HDAC fluorometric assay buffer (50 mM Tris/Cl, pH 8.0, 137 mM sodium chloride, 2.7 mM potassium chloride, and 1 mM magnesium chloride), 15 μL of nuclear extract, and 25 μL of 1 mM acetylated Fluor de Lys substrate. The plates were incubated for 3 h at 37 °C. Subsequently, 50 μL of Fluor de Lys developer solution containing TSA was added to each well, and the plate was incubated for an additional 5 min with gentle shaking at r.t. Readings were collected at an excitation wavelength of 360 nm, and the emitted light was detected at 460 nm using a Tecan microplate reader (BioTek). Negative controls with buffer only and positive controls with HeLa extract in place of inhibitor were performed in the same manner as described above.

2.4. Western blot analysis

Cells were harvested in RIPA lysis buffer (Biosesang) containing protease inhibitors and phosphatase inhibitors (Thermo Fischer). After cell lysis, each sample was centrifuged at 14,000 rpm for 20 min. The supernatant was harvested, and the protein concentration was normalized using the BCA assay (Thermo Fischer). The prepared samples were analyzed by SDS-PAGE and then, following a western blotting procedure, the proteins were transferred to a PVDF membrane and blocked with 5% bovine serum albumin (BSA; Biosesang) in a solution of Tris-buffered saline with Tween 20 (TBST; Biosesang) for 1 h. The membrane was incubated with the primary antibody in TBST at 4 °C

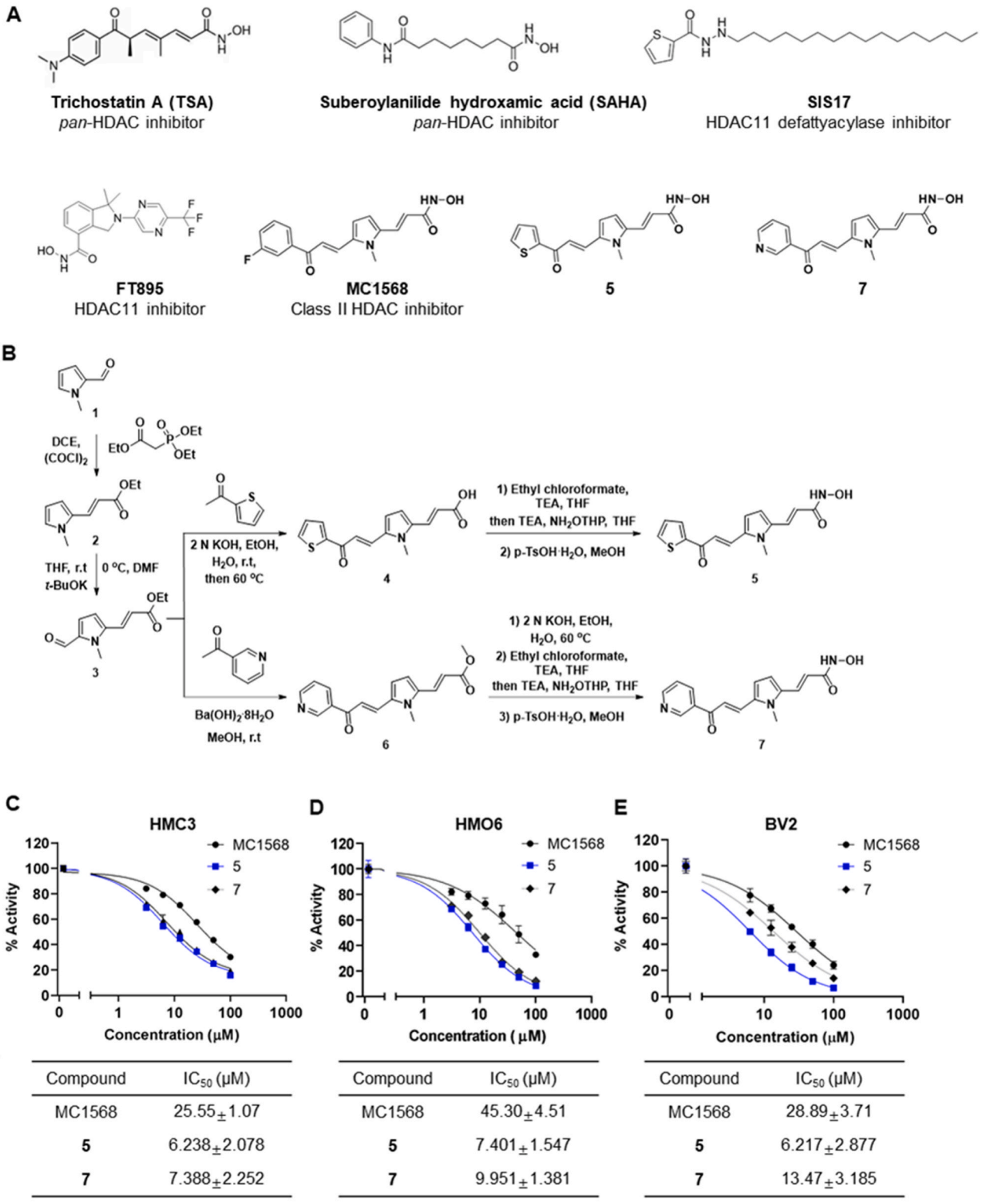

Compound	IC_{50} (μM)
MC1568	$25.55_{\pm}1.07$
5	$6.238_{\pm}2.078$
7	$7.388_{\pm}2.252$

Compound	IC_{50} (μM)
MC1568	$45.30_{\pm}4.51$
5	$7.401_{\pm}1.547$
7	$9.951_{\pm}1.381$

Compound	IC_{50} (μM)
MC1568	$28.89_{\pm}3.71$
5	$6.217_{\pm}2.877$
7	$13.47_{\pm}3.185$

Fig. 1. Development of new HDAC inhibitors. (A) Structures of known and newly designed HDAC inhibitors. (B) Scheme for the synthesis of **5** and **7**. (C-E) Evaluation of cellular histone deacetylase (HDAC) activity in microglia. *pan*-HDAC activity was measured by individual compound treatment using nuclear extracts of HMC3, HMO6, and BV-2 cells. Graphs show mean and standard deviation (SD) values.

overnight, followed by washing with TBST. Primary antibodies used include: anti-Actin (1:3000, 4970 S; CST), anti-LC3 (1:1000, 3868 S; CST), anti-p62 (1:1000, 39749 S; CST), anti-iNOS (1:1000, 13120 S; CST), anti-mTOR (1:1000, 2983 S; CST), anti-pmTOR (1:1000, 5536 S; CST), anti-pS6K (1:1000, 9204 S; CST), and anti-HDAC11 (1:1000, PA5–11249; Invitrogen). Then, the membrane was incubated with a secondary antibody (1:3000, 7074 S, CST) at r.t for 1 h, followed by washing with TBST. Finally, the membrane was developed with an ECL prime solution (Amersham), and chemiluminescence signals were analyzed using ChemiDoc (Bio-Rad).

2.5. Griess assay

NO production was assayed by measuring the nitrite concentration in the supernatant of cultured BV-2 cells. Cells were seeded at a density of 3×10^5 cells/mL in 384-well plates and incubated overnight. The cells were stimulated with 100 ng/mL of lipopolysaccharide (LPS; Sigma–Aldrich) in the absence or presence of test compounds for 24 h, after which they were briefly centrifuged. The supernatant was mixed with an equal volume of Griess reagent (1% sulfanilamide, 0.1% naphthyl ethylenediamine dihydrochloride, and 2.5% H_3PO_4, Sigma–Aldrich) and incubated at r.t for 15 min. Nitrite concentrations were determined by measuring the absorbance of the supernatant at 560 nm. Sodium nitrite ($NaNO_2$) was used to generate a standard curve. Cell viability was determined by measuring the luminescence, which was accomplished by adding 20 μL of Cell Titer Glo reagent (Promega) to the cells and incubating them at r.t for 10 min avoiding direct light. The luminescence signal was measured using a Tecan microplate reader (BioTek). Each value was normalized by the value of DMSO-treated cells.

2.6. Immunofluorescence

Cells were seeded in a confocal dish and maintained for 1 d. The cells were stimulated with 200 ng/mL of LPS (Sigma–Aldrich) in the absence or presence of test compounds for 24 h. After aspirating the media and washing with PBS, 200 μL of a 100% ice-cold MeOH solution was added and the cells were incubated at − 20 °C for 5 min. The solution was then aspirated and the sample was washed with phosphate-buffered saline (PBS) three times. For permeabilization to enable antibody binding, 300 μL of 0.1% Triton-X-100 in PBS solution was added and incubated at r.t for 15 min. The solution was then removed, and the sample was washed with PBS three times. Samples were blocked with 2% BSA in a PBS solution at r.t for 1 h, and the solution of 2% BSA in PBS was then removed and the primary antibody solution of 1% BSA in PBS was added for overnight treatment at 4 °C. The antibody concentration was optimized according to the manufacturer's instructions. The primary antibody solution was removed, and the sample was washed with PBS three times. The secondary antibody solution of 1% BSA in PBS was incubated at r.t for 1 h. Next, the antibody solution was aspirated and the sample was washed with PBS three times. For nuclear staining, Hoechst 33342 was diluted in PBS, added to each well, and incubated at r.t for 5 min. Hoechst 33342 was then removed and the chamber was filled with PBS for subsequent imaging with a microscope.

2.7. Enzyme-linked immunosorbent assay

Cell culture supernatants were collected and assayed for cytokines. The levels of tumor necrosis factor-α (TNF-α) were quantified using enzyme-linked immunosorbent assay (ELISA) kits (R&D Systems). The experiments were performed according to the manufacturer's instructions. In brief, 96-well microplates (R&D Systems) were coated overnight at r.t with capture antibody diluted in PBS without carrier protein, followed by washing with a wash buffer (0.05% Tween 20 in PBS, pH 7.2–7.4) using a microplate washer (BioTek). Microplates were blocked by adding reagent diluent (1% BSA in PBS, pH 7.2–7.4, 0.2 μm filtered) and incubated at r.t for 1 h, followed by washing with the wash buffer. Samples or standards were added to each well and incubated for 2 h at r.t, followed by washing with the wash buffer. The detection antibody was diluted in reagent diluent and then added to each well and incubated for 2 h at r.t, followed by washing with the wash buffer. Streptavidin-HRP was added to each well and incubated for 20 min at r.t avoiding direct light, followed by washing with the wash buffer. TMB solution (Biosesang) was added to each well and incubated for 20 min at r.t avoiding direct light. Subsequently, a stop solution (2 N H_2SO_4) was added to each well and the optical density of each well was immediately determined using a Tecan microplate reader (BioTek) set to 450 nm.

2.8. In vitro HDAC activity assay

Activity assays for individual HDAC isoforms were performed by Eurofins using fluoro-lysine [15]. Human recombinant HDAC6 and 8 were incubated with 25 μM and 400 μM of a fluorogenic HDAC substrate for 30 min at r.t. Human recombinant HDAC11 was incubated with 50 μM of a fluorogenic HDAC substrate (class IIa) for 30 min at 37 °C. The analysis was performed using Hill software developed by Cerep.

2.9. Cellular thermal shift assay

BV-2 cells were seeded in 100-mm culture dishes and incubated overnight. The cells were stimulated with 50 μM of compound for 3 h in the 5% CO_2 incubator at 37 °C. After compound treatment, the cells were washed with PBS and harvested. Distributed each cell suspension, i.e., with DMSO control or with the test compound, into 0.2-mL PCR tubes with 80 μL of cell suspension in each tube. The aliquot of cell suspension was heated for 3 min with the indicated temperature using thermal cycler (Bio-Rad). Then heated cell suspension were lysed by RIPA buffer (Biosesang) and lysates were analyzed by western blot analysis.

2.10. RT-PCR analysis

Cellular mRNA was prepared using NucleoSpin RNA Plus (Macherey-Nagel) according to the manufacturer's instructions. The prepared RNA (1000 ng) from each sample was subjected to reverse transcription at 25 °C for 5 min, 42 °C for 30 min, and 85 °C for 5 min. The cDNA product was mixed with IQ SYBR Green Supermix (Bio-Rad) and individual primers (Bioneer) for RT-PCR analysis using a real-time thermal cycler (Bio-Rad, CFX Connect). *GAPDH* was used as a housekeeping gene to normalize mRNA levels. The following primer sequences were used: human *HDAC6*: forward, 5′-GCCTCAATCACTGAGACCATCC-3′; reverse, 5′-GGTGCCTTCTTGGTGACCAACT-3′; human *HDAC8*: forward, 5′-TGTGCTGGAAATCACGCCAAGC-3′; reverse, 5′-TGTGCTGGAAATCACGCCAAGC-3′; human *HDAC11*: forward, 5′-CTTCTGTGCCTATGCGGACATC-3′; reverse, 5′-GAAGTCTCGCTCATGCCCATTG-3′; human *GAPDH*: forward, 5′-AGGGCTGCTTTTAACTCTGGT-3′; reverse, 5′-CCCCACTTGATTTTGGAGGGA-3′.

2.11. Animal studies

All animal experiments were performed according to guidelines approved by the Institutional Animal Care and Use Committee (IACUC) of the Korea Institute of Science and Technology (KIST, KIST-2021–01–012). ICR mice were obtained from Daehan Bio Link (DBL, South Korea) and housed under controlled conditions of a 12 h light/dark cycle at standard temperature (22 ± 2 °C) with 50 ± 5% humidity and provided with food and water *ad libitum* throughout the study. All mice were acclimated 1 week prior to the beginning of the experiments and were handled daily for at least 3 days before the initiation of the behavior test. The day before every test began, 31–33 g mice were injected intraperitoneally (i.p) with either saline or HDAC inhibitor **5** (50 mg/kg). After 1 h, mice were injected intravenously (i.v) with either saline or LPS (1 mg/kg) to induce a depression-like state following a

previous study with slight modifications [16]. After injection, the mice were moved to individual cages that were 10 cm wide, 27 cm high, and 13 cm deep.

2.12. Immunohistochemistry

Animals were perfused with cold 4% paraformaldehyde (4% PFA; Biosesang). Before perfusion, animals were anesthetized with 15% (w/v) urethane solution intraperitoneally (i.p). Isolated brains were incubated with PFA for 2 h at 4 °C, and transferred to 30% sucrose solution. Samples were cut at 10 μm thickness by cryo-section (Leica CM1860). After pre-treating with solution (40% MeOH, 1.2% H_2O_2 in distilled water) for 15 min, sections were incubated in blocking solution (10% normal chicken serum, 0.6% Triton X-100 in PBS) for 2 h. For the primary antibodies, sections were incubated with goat anti-Iba1 (1:500, PA5–18039; Invitrogen) overnight at 4 °C, then washed with 0.01 M PBS two times before secondary antibody labeling. Following incubating the secondary antibody (1:1000, A11055; Invitrogen) for 1 h, sections were fixed by mounting medium with DAPI (H-1800; VECTASHIELD). Imaging was conducted by Nikon Eclipse TS2 microscope with 20 x objective lens.

2.13. Tail Suspension Test (TST)

TST was performed using a previously described method with slight modifications. The box was 44 cm high, 14 cm wide, and 14 cm deep. To prevent the animals from observing or interacting with each other, each mouse was suspended within its own three-walled rectangular compartment. A suspension ring that was used to suspend the tail of each mouse was positioned at the top of the box. A 17 cm fragment of tape was cut and a length of 2 cm from one end was marked. This 2 cm portion of the tape was attached to the end of the tail, while the remaining 15 cm was used for the suspension of the mouse; the tape adhered to both the mouse's tail and the suspension ring. For the animal behavior observations, all procedures were conducted before 3 p.m. Video was recorded for a total of 8 min, but we only used the portion between 2 min and 8 min for immobility analysis. The definition of immobility in the TST is the center point of the mouse remaining constant as it hangs without struggling. The immobility time was determined using an EthoVision video tracking system (Noldus Information Technology, Wageningen, The Netherlands.

2.14. Forced Swimming Test (FST)

FST was performed following the method introduced in a previous study with slight modifications [17]. The dimensions of the cylinder were 20 cm in height and 10 cm in diameter, and it was filled with water (21–23 °C) to a depth of 15 cm. The water in the cylinder was changed after testing each mouse. For the animal behavior observations, all procedures were conducted before 3 p.m. Video was recorded for a total of 6 min, but only the portion of 2–6 min was used for immobility analysis. The definition of immobility in the FST is the mouse floating in the water, without struggling, making only the movements necessary to keep its head above the water. The counting immobility time was determined using the EthoVision video tracking system.

2.15. Sucrose Preference Test (SPT)

SPT was carried out twice during the behavioral experiments in the mice home cages. One day before the LPS injection, the mice were first habituated to a solution of 14 mL of water and 1% sucrose for 24 h that was contained in a 15 mL tube with a ball nozzle. The day after the TST and FST, the SPT was performed for 24 h. The consumption of water and sucrose by each mouse was measured by weighing their fluid intake on an absolute basis (sucrose and water intake separately). Sucrose preference was calculated using the following formula: sucrose preference ratio (%) = sucrose intake (G) / [sucrose intake (G) + water intake (G)] × 100%. Anhedonia was defined as a reduction in the sucrose preference ratio relative to the control group in the SPT.

2.16. small-interfering RNA (siRNA) Transfection

For gene knockdown, siRNAs were transfected with lipofectamine RNAiMAX reagent (Thermo Fisher) following the manufacturer's protocol, then incubated for 24 h in the 5% CO_2 incubator at 37 °C. After transfection, cells were subjected to LPS (100 ng/ml) treatment for 24 h and protein expression was analyzed by western blot analysis. For NO production, the nitrite concentration in the supernatant of cultured medium was analyzed by Griess assay.

3. Results

3.1. Development of new potent HDAC inhibitor

With a structural insight, we designed new HDAC inhibitors based on the modification of a known HDAC inhibitor, MC1568 (Fig. 1A). MC1568 was synthesized according to a reported procedure [18]. The synthetic pathway employed to prepare compounds **5** and **7** is illustrated in Fig. 1B. First, the Horner–Wadsworth–Emmons olefination reaction of **1** with triethyl phosphonoacetate afforded compound **2**, which was followed by the Vilsmeier–Haack reaction using oxalyl chloride and DMF to give aldehyde **3**. Compound **4** was generated through the aldol condensation reaction of compound **3** with 2-acetylthiophene and subsequent saponification using a 2 N KOH solution to hydrolyze the ester moiety. To introduce a hydroxamic acid moiety, compound **4** was converted into an acid chloride followed by coupling with NH_2OTHP and subsequent removal of the THP group by treatment with *p*-TsOH, which provided compound **5**. For the synthesis of compound **7**, compound **3** was subjected to aldol condensation with 3-acetylpyridine in the presence of a base ($Ba(OH)_2$) to afford compound **6**. Subsequent saponification of compound **6** with KOH (2 N) gave an acid intermediate, which converted into an acid chloride that then underwent a coupling reaction with NH_2OTHP. Finally, the THP-protecting group was removed by treatment with *p*-TsOH, providing compound **7**.

With the desired compounds in hand, we evaluated the inhibitory effect of each derivative using a *pan*-HDAC activity assay in a cell-based system using microglial cell lines. The replacement of the *m*-fluorophenyl unit of MC1568 with a thiophenyl (**5**) or pyridinyl (**7**) moiety remarkably improved the potency for HDAC inhibition in HMC3 and HMO6 human microglial cells and BV-2 mouse microglial cells (Fig. 1C–E). Compared to MC1568, these new compounds exhibited 2.1- to 6.1-fold greater potency for cellular HDAC inhibition. Notably, the potency was slightly better with the thiophenyl functional group (**5**) than with the pyridinyl group (**7**) (Fig. 1C–E). None of the compounds showed any remarkable differences according to the cell line (Supplementary Fig. 1).

3.2. New HDAC inhibitors specifically induce autophagy in microglial cells

Because HDACs are known to play a critical role in the regulation of autophagy and homeostasis in the brain, we investigated the effect of HDAC inhibitors on autophagy in human microglia. LC3 cleavage from LC3-I to LC3-II is an early-stage autophagy marker associated with the formation of autophagosomes, then we examined LC3 cleavage upon treatment with MC1568 and new HDAC inhibitors, **5** and **7**.

Despite the IC_{50} ranges of **5** and **7** for cellular HDACs being similar in HMC3 cells (Fig. 1C), only **5** induced the conversion of LC3-II in HMC3 cells, while no effects were noted with MC1568 or **7** (Fig. 2A). Interestingly, all three compounds had a marginal effect on LC3 cleavage in HMO6 cells (Fig. 2A). For the further validation, we confirmed cell type-specific LC3 conversion by **5** treatment using a dose-dependent

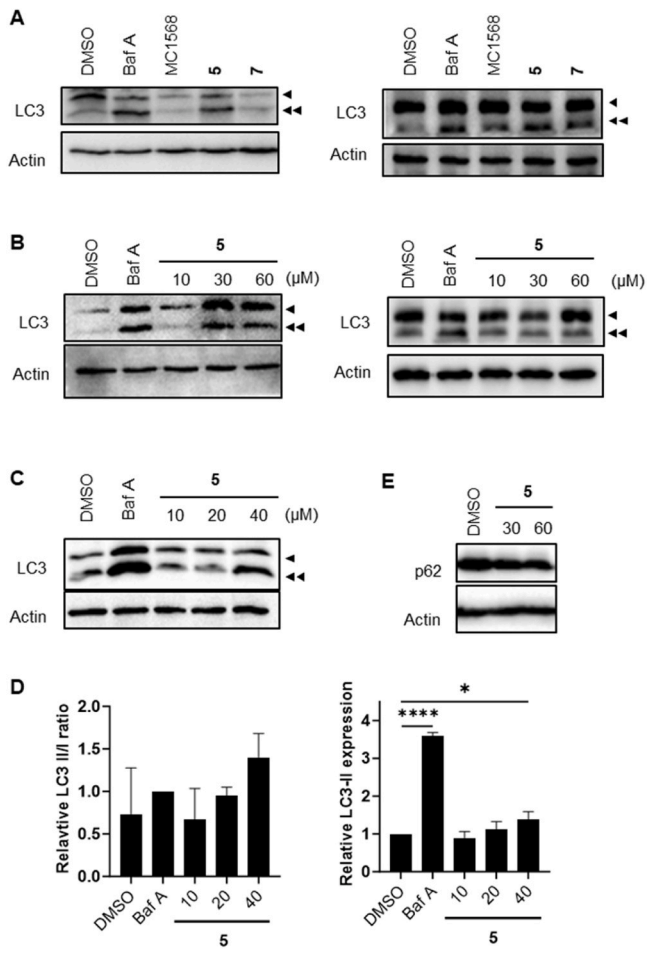

Fig. 2. Regulation of autophagy process by HDAC inhibitor in microglia. (A) Western blot analysis of LC3. HMC3 (left) and HMO6 (right) cells were treated with 60 μM of the indicated compound for 20 h or 10 h. (B) Dose-response tests of **5** for LC3 in HMC3 and HMO6. (C) Dose-response effect of **5** on LC3 in BV-2 cells for 24 h. The arrowhead indicates LC3-I and the double arrowhead indicates LC3-II (left). Bafilomycin A1 (Baf A, Vacuolar H^+-ATPase inhibitor, 40 nM) was used as a positive control. (D) Densitometry graph of western blot analysis in C. LC3 II/I ratio (left) and LC3 II expression (right). *; $P < 0.05$, ****; $P < 0.0001$ by t-test (E) Western blot analysis of p62 in BV-2 cells treated with 10 μM of compound **5** for 24 h.

evaluation, where **5** clearly increased the LC3-II levels in HMC3 cells, and no effect was observed in the HMO6 cells (Fig. 2B). To evaluate whether **5**-induced LC3 conversion particularly observed in HMC3 cells, we examined the effect of **5** in BV-2 cells, where it also increased the LC3-II (Fig. 2C and D). For the clarification of the effect on autophagy flux, we investigated the p62 level as a cargo protein for late-stage autophagy marker, and then validated the decrease in p62 level by autophagic degradation upon **5** treatment (Fig. 2E). From these data, we determined that only **5** specifically initiated autophagy in certain microglia cells, which was unexpectedly not consistent with cell-based *pan*-HDAC inhibition.

3.3. 5 Inhibits LPS-mediated microglial activation by suppressing RNS generation

The generation of RNS such as NO, nitrite, or peroxy-nitrite is critical for the activation of microglia and the promotion of neurotoxicity by neuroinflammation [19]. Considering the anti-inflammatory effect of *pan*-HDAC inhibition [20], we investigated whether MC1568 and new HDAC inhibitors, **5** and **7**, regulate the RNS system by measuring LPS-induced NO production in microglia. Due to the inconsistent range of inflammatory response of immortalized human microglial cell lines [21], we investigated BV-2 mouse microglial cells that robustly increased NO production in response to LPS.

Interestingly, only **5** inhibited LPS-induced NO production in microglia (Fig. 3A). The same structure–activity relationship (SAR) results were observed in the LPS-mediated NO production when monitoring autophagy. In response to LPS, **5** effectively suppressed RNS generation, but **7** did not, despite the two providing similar HDAC inhibitory effects in cells (Fig. 1E). To confirm whether the suppression

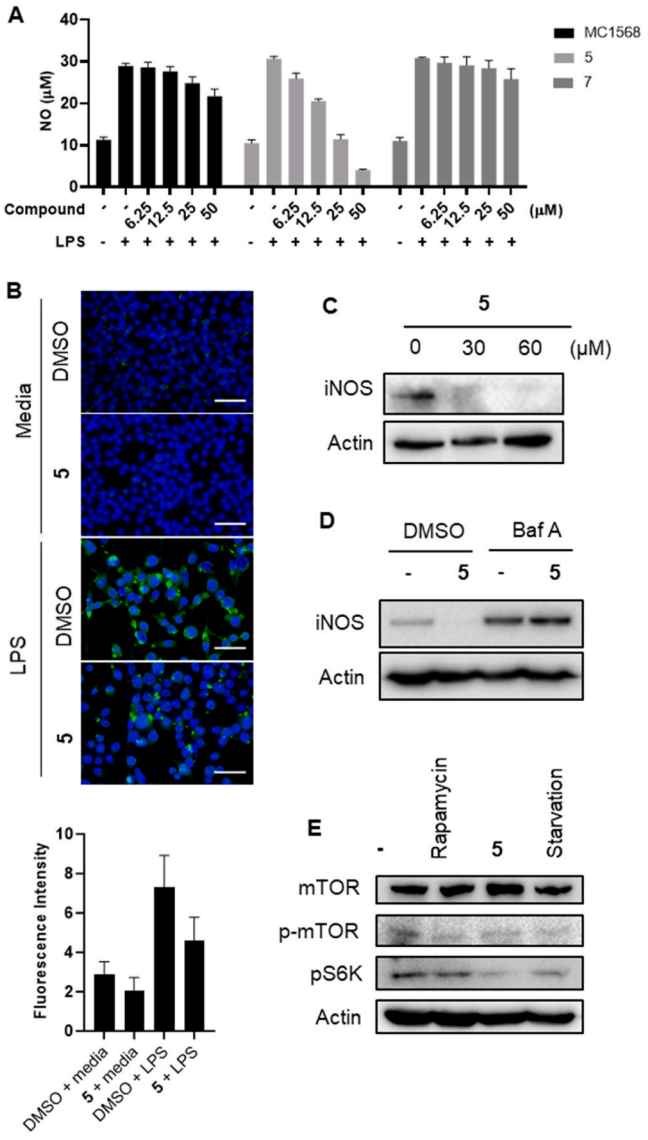

Fig. 3. Anti-neuroinflammatory effect of **5** by inducing autophagy signaling through HDAC inhibition. (A) Griess assay for monitoring NO production. BV-2 cells were pre-treated with indicated concentrations of MC1568, **5**, or **7** for 1 h, and then treated with lipopolysaccharide (LPS; 100 ng/mL) for 24 h. Graphs show mean and SD values. (B) Immunofluorescent images of BV-2 cells. Cells were pre-treated with **5** or DMSO for 1 h, and then treated with LPS (200 ng/mL) for 24 h. Green: anti-Iba1, Blue: Hoechst. The scale bar is 50 μm. Quantification graph for green fluorescent intensity about approximately 100 cells from three experiments. (C) Western blot analysis of inducible NOS (iNOS). BV-2 cells were treated with 30 and 60 μM of **5** for 24 h. (D) Western blot analysis of inducible NOS (iNOS) by inhibition of autophagy flux with Baf A. BV-2 cells were treated with 40 μM of **5** and 20 nM of Baf A for 24 h. (E) Western blot analysis of mTOR signaling pathway. BV-2 cells were treated with 40 μM of compound **5**, 100 nM of rapamycin, and medium without serum for 24 h. Starvation indicated serum starvation.

of NO indeed affects the activation of microglia, we monitored the Iba1 as a marker for microglial activation. By treatment of **5**, LPS-induced microglial activation was clearly decreased in BV-2 cells confirmed by Iba-1 staining (Fig. 3B). However, the LPS-induced TNF-α secretion, which is one of the common pro-inflammatory cytokines, was not suppressed by **5** treatment (Supplementary Fig. 2). Previous studies have shown that *pan*-HDAC inhibitors such as SAHA and VPA mostly suppressed the production of pro-inflammatory cytokines, TNF-α and IL-6, as well as NO in LPS-treated microglia [22]. Based on these findings, we assumed the RNS-generating process as a specific regulatory mechanism of **5** distinct from other HDAC inhibitors and further examined the inducible nitric oxide synthase (iNOS) level in BV-2 cells. It was demonstrated that **5** clearly reduced the protein level of iNOS, not the mRNA level of iNOS by **5** treatment (Fig. 3C and Supplementary Fig. 3). Because **5** particularly induced autophagy in microglia, we tested whether **5**-mediated autophagy decreased the protein level of iNOS. Blocking late autophagy process using Bafilomycin A1 recovered **5**-induced iNOS degradation (Fig. 3D). We further monitored the canonical signaling pathway of autophagy. It was confirmed that **5** induced autophagy by inhibiting mTOR signaling pathway (Fig. 3E). These results indicated that **5**-induced autophagic flux maintained RNS homeostasis by degradation of iNOS in microglia.

3.4. *HDAC11 as responsible isoform for desired cellular phenotype of **5***

The lack of correlation between HDAC enzymatic function and cellular phenotype such as autophagy and NO production in the SAR study led us to explore the activity of MC1568 analogs for individual HDAC isoforms. Through *in vitro* profiling against 11 different HDACs, we established that all three compounds exhibited inhibitory effects on HDAC6, HDAC8, and HDAC11. Notably, MC1568 and compound 5 displayed higher selectivity compared to compound **7**, which inhibited the majority of HDAC isoforms at high dose concentrations (Table 1).

Surprisingly, of the three HDAC isoforms – HDAC6, 8, and 11, the inhibitory pattern of HDAC11 was completely identical to the SAR results of LC3 conversion in HMC3 and LPS-mediated NO suppression in BV-2. The IC_{50} (μM) values of MC1568, **5**, and **7** towards HDAC11 were 21, 1.2, and 22, respectively (Table 1). These results indicated that cellular response for initiating autophagy and attenuating RNS generation phenocopied the inhibition of HDAC11. *In vitro* dose–response graphs of compounds **5** and **7** regarding HDAC6 and 8 were very similar, with 0.7- and 0.94-fold differences of IC_{50} values for HDAC6 and 8, respectively (Fig. 4A). Contrastingly, the activity of the two compounds (**5** and **7**) was highly distinguishable with respect to HDAC11, where an 18-fold difference was observed in their IC_{50} values (Fig. 4A). Based on these results, we identified that HDAC6, 8, and 11 were binding targets of **5**. Among them, we assumed that HDAC11 was the major functional target of **5** for regulating autophagy and RNS in microglia.

Table 1
Activity profiling for HDAC isoforms[a].

HDAC	MC1568	5	7
HDAC1	N.C[†]	N.C	N.C
HDAC2	N.C	N.C	N.C
HDAC3	N.C	N.C	> 30[b]
HDAC4	N.C	N.C	> 30
HDAC5	N.C	N.C	> 30
HDAC6	8.4 ± 1.1[c]	0.78 ± 1.09	0.54 ± 1.05
HDAC7	N.C	N.C	> 30
HDAC8	18.2 ± 1.1	1.0 ± 1.1	0.94 ± 1.1
HDAC9	N.C	N.C	N.C
HDAC10	N.C	N.C	> 30
HDAC11	21.4 ± 1.3	1.2 ± 1.3	22 ± 1.3

[a] IC_{50} (μM) value of each compound. Human recombinant HDAC enzymes were used for *in vitro* activity profiling. The assays were performed with concentrations of 0.3–30 μM of each HDAC inhibitor and the respective reference compound was tested concurrently. Trichostatin-A (TSA) for HDAC1–10 and scriptaid for HDAC11 were used as reference compounds. The IC_{50} values of TSA for HDAC1–10 were measured to be 5.3 × 10–9–4.7 × 10–6 M and the IC_{50} value of scriptaid for HDAC11 was measured as 5.6 × 10–6 M.; †N.C: IC_{50} value not calculable with less than 25% inhibitory effect at 30 μM.;
[b] > 30: IC_{50} value above 30 μM with less than 50% inhibitory effect at 30 μM.;
[c] IC_{50} values show mean and error.

Overall evidence such as **5**-specific SAR results for autophagy and RNS regulation, *in vitro* enzyme activity, direct binding of **5** with HDAC11, and HDAC11-high cell-type-specific phenotype of **5** suggested that HDAC11 is mainly responsible for the desired phenotype of **5** in microglia. Therefore, we concluded that HDAC11 plays a critical role in **5**-mediated autophagy and RNS in microglia.

3.5. ***5** Inhibits deacetylase function of HDAC11*

HDAC11, as the sole class-IV HDAC, has been reported to exhibit characteristic properties such as defatty-acylase activity towards serine hydroxymethyl transferase 2 (SHMT2) as well as deacetylase [23]. It should be noted that the HDAC profiling performed in this study works for deacetylase function using a fluorogenic acetylated peptide substrate (Table 1). This result suggested the possibility that **5** inhibits the deacetylase function of HDAC11. For further validation, we confirmed **5** as a deacetylase inhibitor of HDAC11 because the acetylation level of histone 3 (H3) was clearly increased in **5**-treated cells (Fig. 4C).

To elucidate the mechanism of action for **5**-inhibited RNS generation, we evaluated the pharmacological effects of **5**, SIS17, and FT895 on LPS-induced NO production. SIS17 is a known HDAC11 inhibitor that selectively inhibits de-myristoylation rather than deacetylation, while FT895 inhibits deacetylation of H3 [13,24]. Upon comparing the *in vitro* IC_{50} values of **5** (1.2 μM, Table 1), SIS17 [13] (0.83 μM), and FT895 [25] (0.74 μM) towards HDAC11, SIS17 hardly showed inhibition for NO-releasing despite their similar dosage ranges (Fig. 4D). We further investigated the effect of SIS17 on autophagy initiation, then SIS17 showed a marginal effect on LC3 cleavage (Fig. 4E). Furthermore, a previous study reported that HDAC11 down-regulated type I interferon (IFN) response through a defatty-acylation of SHMT2 [14]. We measured the effect of SIS17 and **5** on the secretion of IP-10, one of the type I IFN cytokine, by stimulation of type I IFN signaling, then only SIS17 enhanced IP-10 secretion, not **5** (Supplementary Fig. 7). All these results indicated that deacetylase and defatty-acylase functions of HDAC11 distinctly controlled the particular biological phenomena. Our finding indicated that the inhibition of deacetylase function of HDAC11 attenuated RNS generation in microglia.

To verify whether HDAC11 is the direct target of **5** at the cellular level, we performed a cellular thermal shift assay. In response to increasing temperature, a thermal stability of protein is perturbed. Once it binds to protein, the compound provides a structural stability and the thermal stability of target protein would be shifted. We examined the thermal stability of HDAC11 with or without **5** treatment in BV-2 cells. Proteins were denatured by increasing temperature in DMSO control, whereas the interaction of HDAC11 with **5** induced toleration against denaturation of HDAC11 by extra thermal stability (Supplementary Fig. 4). Furthermore, we investigated the loss-of-function effect using HDAC11 knock-down (KD) in BV-2 cells. Even though si-HDAC11 transfection was not highly efficient and exhibited an impact on the basal status of BV-2 cells, the KD of HDAC11 induced the inhibition of LPS-induced NO-releasing and the increase of LC3 cleavage in BV-2 cells (Supplementary Fig. 5 and 6). Due to the low KD efficiency, **5** still induced LC3 conversion in si-HDAC11 transfection, nevertheless its potency was reduced compared to control transfection (Supplementary Fig. 6). These cellular evidences supported HDAC11 as a cellular binding target of **5** in microglia cells. To further confirm the relationship between HDAC11 and the cell type-specific effect of **5** in human microglia, we examined the gene expression levels in both HMC3 and HMO6 cells. As expected, the RNA expression level of HDAC11 in HMC3 cells was upregulated compared to that in HMO6 cells, while no substantial differences were observed between their HDAC6 and 8 levels (Fig. 4B).

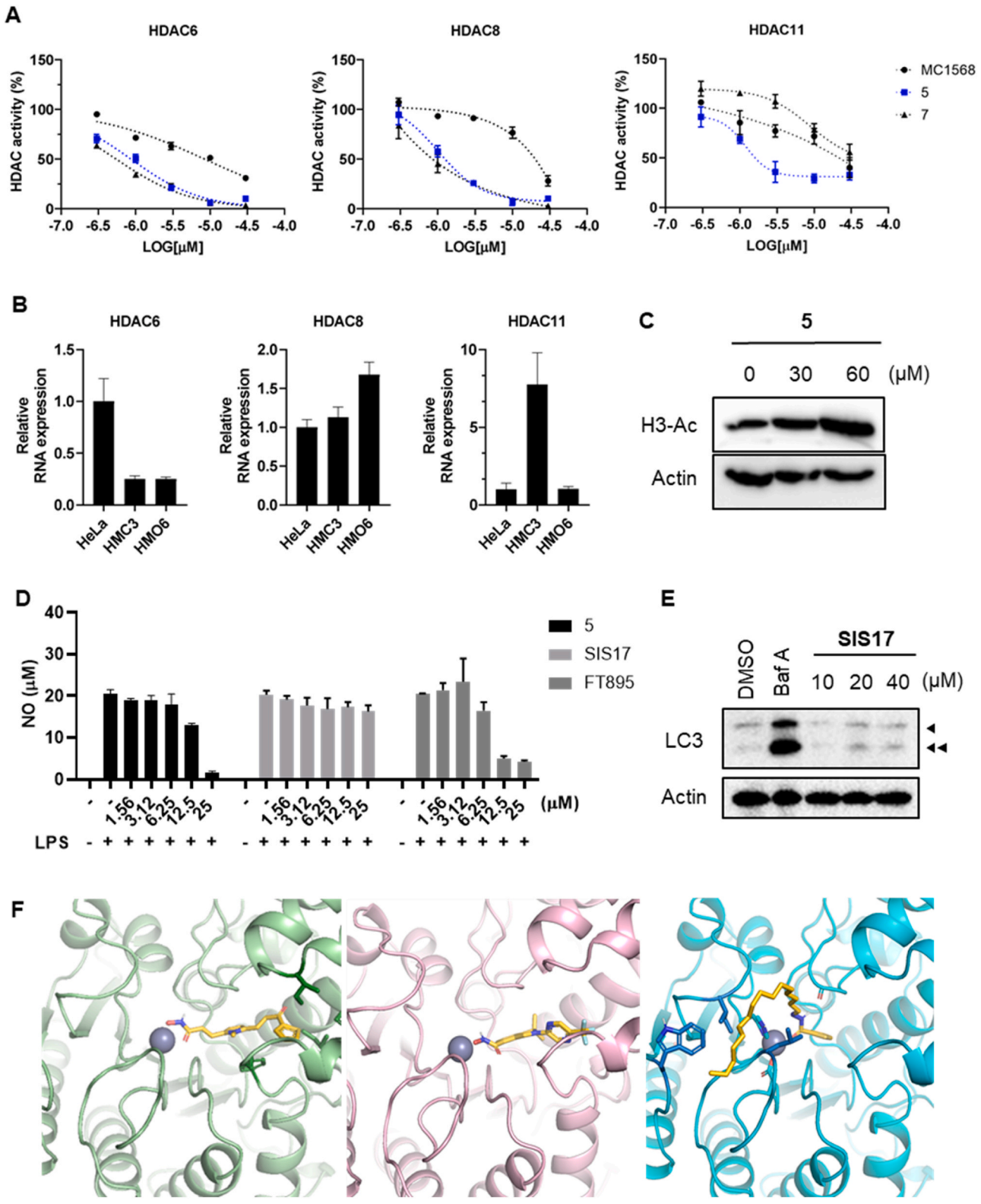

Fig. 4. **5** inhibits deacetylase function of HDAC11. (A) *In vitro* activity for HDAC6, HDAC8, and HDAC11 upon treatment with individual HDAC inhibitors. HDAC activity was calculated as the percentage of the control-treated enzyme activity. Graphs show mean and SD values. (B) Gene expression for HDAC isoforms in human microglia cells. Relative expression levels for the RNA of HDAC6, HDAC8, and HDAC11 were measured by HMC3 and HMO6 cells. HeLa was used for a comparison of the relative levels. Relative quantification (RQ) was normalized by GAPDH as an internal standard. Graphs depict mean and RQmax values. (C) Western blot analysis of H3-Ac. BV-2 cells were treated with 30, and 60 μM of compound **5** for 24 h. (D) BV-2 cells were pre-treated with indicated concentrations of SIS17, FT895, or **5** for 1 h, and then treated with LPS (100 ng/mL) for 24 h. Production of NO in the conditioned media was determined using Griess assay. Graphs show mean and SD values. (E) Western blot analysis for LC3 by treatment of SIS17. BV-2 cells were treated by SIS17 of the indicated concentration for 24 h. (F) Molecular docking study. Complex models of **5** (left), FT895 (middle), and SIS17 (right) molecules docked to the human HDAC11 AlphaFold model. Ligand molecules are prepared and docked using Rosetta GALigandDock following the standard receptor-flexible protocol. Energy minimum structures are shown in the figures.

Computational analysis for chemical structures and small molecule-HDAC11 interaction also supported the different biological activity between **5** and SIS17. 3D conformer generation provided the molecular similarity of three compounds, **5**, SIS17, and FT895 which resulted in SIS17 having quite different structural similarity compared to **5** and FT895 with the distinguished number of conformers (Supplementary Table 1). We further investigated the binding mode for three compounds, **5**, SIS17, and FT895 against HDAC11 by molecular docking study. Because no crystal structure for HDAC11 has been available so far, we utilized the AlphaFold model of HDAC11 (Supplementary Fig. 8). Corresponding to the chemical structure analysis, the binding modes of **5** and FT895 with HDAC11 were similar, whereas SIS17 showed distinct interaction based on the flexible lipid chain. In the predicted complexes for **5** and FT895, ligands are buried inside the N-terminus part of the receptor (right-hand side to the zinc), while in the SIS17 complex, the ligand is exposed to the surface and stacked at the exposed hydrophobic patch (Fig. 4E, highlighted in dark blue color). Structural similarity and docking analysis suggested the different mode-of-action between **5** and SIS17 for HDAC11. The distinct binding modes between **5** and SIS17 would regulate the different activity for HDAC11. Based on the pharmacological and computational analysis, therefore, we concluded that the desired phenotype mediated by **5** resulted from its disruption of the deacetylase function of HDAC11.

3.6. Protective effect of depressive-like symptoms by 5

CNS homeostasis by microglia is critical for regulating cognitive function in brain [26]. There exists growing evidence regarding the correlation between microglial activation and various pathological conditions, including immunological, physiological, and psychological stress [27]. Recent studies and growing clinical evidence have suggested that depression is considered a microgliopathy [28]. Furthermore, endotoxin-induced neuroinflammation is a well-known animal model used to study the acute effects of depressive-like behavior in mice [29]. Regarding the important role of HDAC-mediated microglial activation, we investigated the anti-depressant activity of **5** in response to LPS treatment in mice.

To validate the microglia-mediated anti-neuroinflammation of **5** *in vivo* system, we first examined whether **5** altered the microglial activation in mouse brain. Because microglia are found in various regions of the brain, we monitored the LPS-induced microglial activation throughout the brain by Iba-1 staining. As we expected, administration of **5** reduced LPS-induced microglial activation in most brain regions such as the amygdala, prefrontal cortex (PFC), hippocampus (HIP), anterior cingulate cortex, ventral tegmental area, and olfactory bulb (Fig. 5A and Supplementary Fig. 9). In particular, the amygdala, PFC, and HIP are known regions where microglia are activated in the status of depression, and administration of **5** inhibited the activation of microglia by LPS in all three regions [30].

With the desired response of **5** in immunohistochemistry of mice brain, we performed the tail suspension test (TST) and forced swimming test (FST) to monitor behavioral despair, and the sucrose preference test (SPT) for monitoring anhedonia to evaluate the pharmacological effect (Fig. 5B). These behavioral tests are widely used to evaluate the pharmacological effects of a drug against stress-evoked depressive-like behavior in rodents [31]. The results showed that mice injected with LPS had significantly increased immobility time in the TST or FST and decreased sucrose preference compared to that of the control group. Interestingly, administration with HDAC inhibitor **5** significantly rescued the LPS-induced depressive-like symptoms in all three behavioral tests. The high immobility times observed for LPS-treated mice in the TST and FST were significantly alleviated upon their treatment with **5** (Fig. 5C and D). In addition, the reduced consumption of sucrose solution induced by LPS treatment was significantly recovered by **5** treatment (Fig. 5E). No remarkable acute toxicity was observed in the **5**-treatment group during the behavioral tests. All these results suggest targeting HDAC11 as a novel therapeutic strategy for microgliopathy and the therapeutic potential of **5** as an antidepressant in animal models.

4. Discussion

Given the fact that HDACs are highly related to autophagy and inflammation response, the pharmacological inhibition of HDACs is being considered a potential therapy by various disease research fields [32]. For example, *pan*-HDAC inhibitors were reported to induce autophagy in cancer cells *via* intrinsic mitochondria or the FOXO1 pathway and they are also known to play an important role in microglial phagocytic capacity and neuroinflammation [33,34]. SAHA also improved autophagic function in Cockayne syndrome group B-deficient mice and induced neuroprotection for ischemia by an anti-inflammatory effect in microglia [5,10]. In addition to *pan*-HDAC inhibitors, class I/II HDAC inhibitor was reported to regulate microglial polarization and mitigate neuroinflammation through the GSK3β pathway, thus preventing traumatic brain injury [22].

Because HDAC11 is mainly expressed in the CNS and the entirety of the brain, where it regulates neural differentiation, it is considered a therapeutic target for psychiatric diseases, such as schizophrenia, as well as depression [35]. Additionally, HDAC11 is considered an attractive target for treating myeloproliferative neoplasm malignant hematopoiesis [24]. Despite significant research efforts, the HDAC11 modulation of autophagy and inflammation processes in microglia remained unclear due to a lack of proper chemical tools for such an analysis. In this study, we developed a potent new HDAC inhibitor **5**, that initiated the autophagy process and reduced NO production in microglia. The selectivity profiling of MC1568 derivatives for HDAC isoforms successfully elucidated the important role of HDAC11 in the regulation of autophagy and RNS in microglia.

The modulation of HDAC11 *via* inhibitor **5** in microglia initiated the autophagy process and induced the clearance of cargo proteins such as iNOS, which is a key mediator of RNS regulation. Based on these results, we assumed that HDAC11-mediated autophagy regulation is distinct from that of other HDAC isoforms. HDAC11 has unique biological functions, that is deacetylation and long-chain deacylation. SIS17 and FT895 are respectively known as defatty-acylase inhibitor and deacetylase inhibitor for HDAC11. The evaluation for SIS17, FT895, and **5** demonstrated that the perturbation of deacetylase function was mainly responsible for autophagy and NO production in microglia (Fig. 2, 4D, and 4E). Structural analysis and binding mode prediction for HDAC11 of three compounds also supported a different regulation of HDAC11 by **5** and SIS17 (Fig. 4E and Supplementary Table 1). Even though **5** inhibited HDAC6, HDAC8, and HDAC11 (Table 1), only HDAC11 was significantly expressed in HMC3 cells (Fig. 4B). Therefore, we concluded that the deacetylase function of HDAC11 is mainly responsible for the RNS regulation of microglia by autophagic degradation of iNOS.

In terms of therapeutic applications, microglia-mediated neuroinflammation has been considered an important mechanism in depression [36]. Behavioral tests for despair and anhedonia in mice demonstrated the therapeutic potential of **5** for antidepressant activity. Note that the complete inhibition of NO production by **5** was sufficient to induce antidepressant activity without the alteration of pro-inflammatory cytokine levels, such as those of TNF-α.

These findings reveal that the development of specific HDAC inhibitors could be a valuable tool for exploring the biological function of HDACs. Further study of the identification of more selective HDAC11 inhibitors may provide an efficient treatment strategy for depressive disorder.

5. Conclusion

Histone deacetylases are epigenetic controllers that play crucial roles in various signaling pathways such as inflammation and autophagy. Among them, HDAC11, which belongs to the recently discovered class

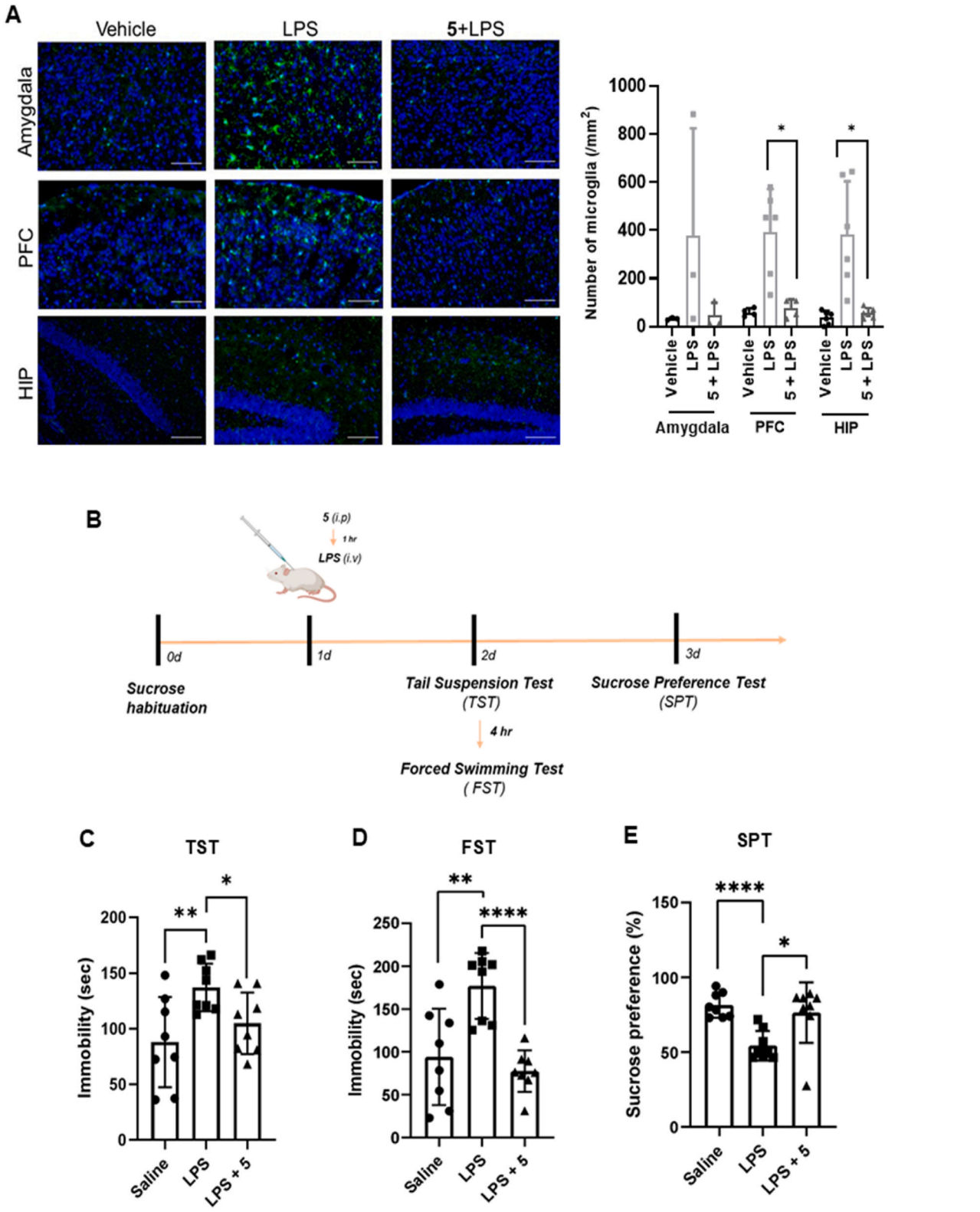

Fig. 5. Immunohistochemistry and behavior test for antidepressant activity of compound **5** in LPS-induced mice. (A) Representative immunohistochemistry images of Iba1 and DAPI staining (left) and quantified graph (right). n = 3–5 mice per experimental group. Sections were visualized with anti-Iba-1 (green) and DAPI (blue). The scale bar is 100 μm. 10 images per animal were analyzed and quantified by the number of microglia per mm^2 at indicated regions. Graphs show mean and SD values. P *<0.05 by two-way ANOVA. PFC: prefrontal cortex, HIP: hippocampus. (B) Schematic workflow of three different behavior tests. Mice were subjected to intraperitoneal treatment of **5** (50 mpk), then intravenously injected with LPS (1 mpk). Behavior tests were performed the next day with a sequence of tail suspension test (TST), forced swimming test (FST), and sucrose preference test (SPT) (C-E). For administration, mice were classified into three different groups (saline, LPS, and co-treatment with LPS and **5** (LPS + **5**)). Immobility time in TST (C) and FST (D) and sucrose preference percentage in SPT (E) were measured for the three different groups. Graphs show mean and SD values; n = 8 for each group. P *<0.05, **< 0.01, ****< 0.0001 by t-test.

IV HDAC and is expressed predominantly in the brain, has received significant attention due to its potential as a key regulator in brain research. In this study, we present a newly designed compound, **5**, that could induce initial autophagy in microglia and degrade the levels of NOS, resulting in the suppression of inflammation and neuroprotection in both human and murine cell lines. Furthermore, our *in vivo* experiments confirmed that the administration of compound **5** could alleviate the symptoms of inflammation-induced depression in mouse models. Our investigation of the role of HDAC11 in microglia provides the potential of HDAC inhibition as an anti-inflammatory strategy for brain disorders. We have elucidated the specific function of HDAC11 and proposed possibilities for targeting HDAC11 in the brain for therapeutic purposes.

Ethics approval and consent to participate

All animal experiments were performed in accordance with the Institutional Animal Care and Use Committee of the Korea Institute of Science and Technology (KIST, KIST-2021–01–012).

CRediT authorship contribution statement

S. Lee: Supervision, Project administration, Conceptualization, Writing – review & editing. **J. Kim:** Supervision, Project administration, Conceptualization, Writing – review & editing. **S. Y. Baek:** Validation, Investigation, Writing – original draft preparation, Visualization, Formal analysis. **J. Lee;** Validation, Investigation, Writing – original draft preparation, Visualization, Formal analysis. **T. Kim;** Validation, Investigation, Visualization. **H. Lee;** Investigation, Visualization. **H-S. Choi;** Data curation, Methodology. **M. Koh;** Investigation. **E. Kim;** Data curation, Investigation. **J-Y. Lee;** Investigation, Resources. **M. E. Jung;** Methodology, Resources. **D. Iliopoulos;** Methodology.

Declaration of Competing Interest

The authors declare no conflicts of interest.

Data availability

Data will be made available on request.

Acknowledgments

This work was supported by the KIST Institutional Program under Grant (Nos. 2E32212, 2V09713 and 2E32164), a National Research Foundation of Korea (NRF) grant funded by the Korean government (NRF-2021R1C1C1005134, 2021R1A6A1A10044154 and RS-2023-00211336), and a research grant from Eli & Edythe Broad Foundation awarded to Prof. Dr. Dimitrios Iliopoulos. HMC3, BV-2, and HMO6 cell lines were kindly provided by Dr. H. Ryu and Dr. K. Park at the Korea Institute of Science and Technology (KIST) and by Prof. S. H. Paek at Seoul National University Hospital.

Appendix A. Supporting information

Supplementary data associated with this article can be found in the online version at doi:10.1016/j.biopha.2023.115312.

References

[1] C. Damaskos, I. Tomos, N. Garmpis, A. Karakatsani, D. Dimitroulis, A. Garmpi, E. Spartalis, C.F. Kampolis, E. Tsagkari, A.A. Loukeri, Histone deacetylase inhibitors as a novel targeted therapy against non-small cell lung cancer: where are we now and what should we expect, Anticancer Res. 38 (1) (2018) 37–43.
[2] M. Parra, E. Verdin, Regulatory signal transduction pathways for class IIa histone deacetylases, Curr. Opin. Pharmacol. 10 (4) (2010) 454–460.
[3] Y. Li, E. Seto, HDACs and HDAC inhibitors in cancer development and therapy, Cold Spring Harb. Perspect. Med. 6 (10) (2016), a026831.
[4] B.S. Durham, R. Grigg, I.C. Wood, Inhibition of histone deacetylase 1 or 2 reduces induced cytokine expression in microglia through a protein synthesis independent mechanism, J. Neurochem. 143 (2) (2017) 214–224.
[5] M. Majora, K. Sondenheimer, M. Knechten, I. Uthe, C. Esser, A. Schiavi, N. Ventura, J. Krutmann, HDAC inhibition improves autophagic and lysosomal function to prevent loss of subcutaneous fat in a mouse model of Cockayne syndrome, Sci. Transl. Med. 10 (456) (2018) eaam7510.
[6] M. Datta, O. Staszewski, E. Raschi, M. Frosch, N. Hagemeyer, T.L. Tay, T. Blank, M. Kreutzfeldt, D. Merkler, S. Ziegler-Waldkirch, Histone deacetylases 1 and 2 regulate microglia function during development, homeostasis, and neurodegeneration in a context-dependent manner, Immunity 48 (3) (2018), 514–529. e6.
[7] A.M. Casano, F. Peri, Microglia: multitasking specialists of the brain, Dev. Cell 32 (4) (2015) 469–477.
[8] L. Gao, M.A. Cueto, F. Asselbergs, P. Atadja, Cloning and functional characterization of HDAC11, a novel member of the human histone deacetylase family, J. Biol. Chem. 277 (28) (2002) 25748–25755.
[9] S.-S. Liu, F. Wu, Y.-M. Jin, W.-Q. Chang, T.-M. Xu, HDAC11: a rising star in epigenetics, Biomed. Pharmacother. 131 (2020), 110607.
[10] S. Li, X. Lu, Q. Shao, Z. Chen, Q. Huang, Z. Jiao, X. Huang, M. Yue, J. Peng, X. Zhou, Early histone deacetylase inhibition mitigates ischemia/reperfusion brain injury by reducing microglia activation and modulating their phenotype, Front. Neurol. 10 (2019) 893.
[11] M. Yoshida, M. Kijima, M. Akita, T. Beppu, Potent and specific inhibition of mammalian histone deacetylase both *in vivo* and *in vitro* by trichostatin A, J. Biol. Chem. 265 (28) (1990) 17174–17179.
[12] A. Saito, T. Yamashita, Y. Mariko, Y. Nosaka, K. Tsuchiya, T. Ando, T. Suzuki, T. Tsuruo, O. Nakanishi, A synthetic inhibitor of histone deacetylase, MS-27-275, with marked *in vivo* antitumor activity against human tumors, Proc. Natl. Acad. Sci. 96 (8) (1999) 4592–4597.
[13] S.I. Son, J. Cao, C.-L. Zhu, S.P. Miller, H. Lin, Activity-guided design of HDAC11-specific inhibitors, ACS Chem. Biol. 14 (7) (2019) 1393–1397.
[14] J. Cao, L. Sun, P. Aramsangtienchai, N.A. Spiegelman, X. Zhang, W. Huang, E. Seto, H. Lin, HDAC11 regulates type I interferon signaling through defatty-acylation of SHMT2, Proc. Natl. Acad. Sci. 116 (12) (2019) 5487–5492.
[15] X. Zhao, F. Cao, Q. Liu, X. Li, G. Xu, G. Liu, Y. Zhang, X. Yang, S. Yi, F. Xu, Behavioral, inflammatory and neurochemical disturbances in LPS and UCMS-induced mouse models of depression, Behav. brain Res. 364 (2019) 494–502.
[16] S. Ostadhadi, N. Kordjazy, A. Haj-Mirzaian, S. Ameli, G. Akhlaghipour, A. Dehpour, Involvement of NO/cGMP pathway in the antidepressant-like effect of gabapentin in mouse forced swimming test, Naunyn-Schmiede 'S. Arch. Pharmacol. 389 (4) (2016) 393–402.
[17] Y. Zhu, E.A. Klomparens, S. Guo, X. Geng, Neuroinflammation caused by mental stress: the effect of chronic restraint stress and acute repeated social defeat stress in mice, Neurol. Res. 41 (8) (2019) 762–769.
[18] C.L. Fleming, T.D. Ashton, V. Gaur, S.L. McGee, F.M. Pfeffer, Improved synthesis and structural reassignment of MC1568: a class IIa selective HDAC inhibitor, J. Med. Chem. 57 (3) (2014) 1132–1135.
[19] H. Takeuchi, Neurotoxicity by microglia: mechanisms and potential therapeutic strategy, Clin. Exp. Neuroimmunol. 1 (1) (2010) 12–21.
[20] I. Adcock, HDAC inhibitors as anti-inflammatory agents, Br. J. Pharmacol. 150 (7) (2007) 829–831.
[21] C. Dello Russo, N. Cappoli, I. Coletta, D. Mezzogori, F. Paciello, G. Pozzoli, P. Navarra, A. Battaglia, The human microglial HMC3 cell line: where do we stand? A systematic literature review, J. Neuroinflamm. 15 (1) (2018) 1–24.
[22] G. Wang, Y. Shi, X. Jiang, R.K. Leak, X. Hu, Y. Wu, H. Pu, W.-W. Li, B. Tang, Y. Wang, HDAC inhibition prevents white matter injury by modulating microglia/macrophage polarization through the GSK3β/PTEN/Akt axis, Proc. Natl. Acad. Sci. 112 (9) (2015) 2853–2858.
[23] C. Moreno-Yruela, I. Galleano, A.S. Madsen, C.A. Olsen, Histone deacetylase 11 is an ε-N-myristoyllysine hydrolase, Cell Chem. Biol. 25 (7) (2018), 849–856. e8.
[24] L. Yue, V. Sharma, N.P. Horvat, A.A. Akuffo, M.S. Beatty, C. Murdun, C. Colin, J. M. Billington, W.E. Goodheart, E. Sahakian, HDAC11 deficiency disrupts oncogene-induced hematopoiesis in myeloproliferative neoplasms, Blood 135 (3) (2020) 191–207.
[25] S.I. Son, D. Su, T.T. Ho, H. Lin, Garcinol is an HDAC11 inhibitor, ACS Chem. Biol. 15 (11) (2020) 2866–2871.
[26] T. Blank, M. Prinz, Microglia as modulators of cognition and neuropsychiatric disorders, Glia 61 (1) (2013) 62–70.
[27] L. Du, Y. Zhang, Y. Chen, J. Zhu, Y. Yang, H.-L. Zhang, Role of microglia in neurological disorders and their potentials as a therapeutic target, Mol. Neurobiol. 54 (10) (2017) 7567–7584.
[28] R. Yirmiya, N. Rimmerman, R. Reshef, Depression as a microglial disease, Trends Neurosci. 38 (10) (2015) 637–658.
[29] V.N. de Paiva, S.N. Lima, M.M. Fernandes, R. Soncini, C.A. Andrade, A. Giusti-Paiva, Prostaglandins mediate depressive-like behaviour induced by endotoxin in mice, Behav. brain Res. 215 (1) (2010) 146–151.
[30] H. Park, G. Zhou, M. Baek, D. Baker, F. DiMaio, Force field optimization guided by small molecule crystal lattice data enables consistent sub-angstrom protein-ligand docking, J. Chem. Theory Comput. 17 (3) (2021) 2000–2010.
[31] K. Belovicova, E. Bogi, K. Csatlosova, M. Dubovicky, Animal tests for anxiety-like and depression-like behavior in rats, Interdiscip. Toxicol. 10 (1) (2017) 40.

[32] E.E. Hull, M.R. Montgomery, K.J. Leyva, HDAC inhibitors as epigenetic regulators of the immune system: impacts on cancer therapy and inflammatory diseases, BioMed. Res. Int. 2016 (2016).
[33] N. Gammoh, D. Lam, C. Puente, I. Ganley, P.A. Marks, X. Jiang, Role of autophagy in histone deacetylase inhibitor-induced apoptotic and nonapoptotic cell death, Proc. Natl. Acad. Sci. 109 (17) (2012) 6561–6565.
[34] J.A. Rodríguez-Gómez, E. Kavanagh, P. Engskog-Vlachos, M.K. Engskog, A. J. Herrera, A.M. Espinosa-Oliva, B. Joseph, N. Hajji, J.L. Venero, M.A. Burguillos, Microglia: agents of the CNS pro-inflammatory response, Cells 9 (7) (2020) 1717.
[35] B.D. Strahl, C.D. Allis, The language of covalent histone modifications, Nature 403 (6765) (2000) 41–45.
[36] H. Liu, Q. Hu, A. Kaufman, A.J. D'Ercole, P. Ye, Developmental expression of histone deacetylase 11 in the murine brain, J. Neurosci. Res. 86 (3) (2008) 537–543.